JOURNAL OF MATERIALS SCIENCE 18 (1983) 3337–3347

Strength–structure relationships in PAN-based carbon fibres

S. C. BENNETT, D. J. JOHNSON
Textile Physics Laboratory, Department of Textile Industries, University of Leeds, Leeds, UK

W. JOHNSON
Materials and Structures Department, Ministry of Defence (PE) Royal Aircraft Establishment, Farnborough, Hants, UK

Type I PAN-based carbon fibres have been stressed to failure in glycerol; this enables the fracture ends to be preserved intact for subsequent examination, first by scanning electron microscopy, then, after embedding and sectioning, by transmission electron microscopy. Internal flaws which did not initiate failure was seen to have walls containing crystallites arranged mainly parallel to the fibre axis. Internal and surface flaws which did initiate failure showed evidence of large misoriented crystallites in the walls of the flaws. It is the presence of misoriented crystallites rather than the flaw itself which determines whether or not tensile failure will occur. Our observations are entirely consistent with the Reynolds–Sharp mechanism of tensile failure in which the concentration of shear energy in a misoriented crystallite is not relieved by cracks parallel to the layer planes but by cracks at right angles. It is possible to predict that, in the absence of gross flaws, breaking strains of 1 to 1.3% should be possible in Type I PAN-based carbon fibres, and greater than 2% in Type II carbon fibres.

1. Introduction

1.1. Defect-limited strength

The structure of a material, and the behaviour of the structural elements under deformational stress, determine its physical properties. With carbon fibres there is a well established correlation between preferred orientation and Young's Modulus [1], but relationships between structural parameters and tensile strength are less certain. It is now well established that strength is gauge-length dependent [2], and that this is a consequence of internal and surface flaws [3, 4]. These flaws have been well characterized by high-voltage and normal-voltage low-resolution electron microscopy [5, 6]; Moreton and Watt [7] demonstrated that flaws may arise from impurity particles in the polyacrylonitrile (PAN) precursor, and that, when minimized by clean-room spinning, carbon fibres can be produced at both 1400 and 2500° C with tensile strengths of around 3 GPa. Fibres with strengths exceeding 3.5 GPa are now available commercially.

Unlike the theoretical Young's modulus, the theoretical tensile strength of a solid is difficult to evaluate [8]. One approach is the Orowan–Polanyi expression $\sigma_t = (E\gamma_a/a)^{1/2}$ which relates the theoretical strength σ_t to Young's Modulus E, the equilibrium surface energy γ_a, and the interplanar spacing a of the planes perpendicular to the tensile axis. The ratio σ/E varies considerably, but for many materials is in the range 0.1 to 0.2. For a perfect graphite, E is approximately 1000 GPa and, consequently, σ_t should be about 100 GPa. Because of defects, the practical strength is always an order of magnitude lower than the theoretical strength, thus, in the most perfect form of fibrous carbon so far produced, the graphite whisker, E is about 680 GPa and σ about 20 GPa [9] giving a σ/E ratio of 0.03. The strongest carbon fibres have σ/E ratios around 0.02. In

0022–2461/83 $03.00 + .12

brittle solids the defects are small cracks which act as stress concentrators, and they grow under the action of a stress σ if they are greater than a critical size C as determined by the Griffiths relationship

$$\sigma^2 = 2E\gamma_a/\pi C \quad (1)$$

If this relationship is applied to a graphite whisker, with $\gamma_a = 4.2\ \mathrm{Jm}^{-2}$, the critical flaw size is 4.5 nm, and for a high-strength carbon fibre ($\sigma = 3.9$ GPa, $E = 230$ GPa) it is 40 nm.

1.2. Reynolds–Sharp theory

The fine structure of most types of PAN-based carbon fibre is now well understood [10–14]. High resolution lattice-fringe images of longitudinal and transverse sections have shown that there is a complex interlinking of layer planes both longitudinally and laterally; this is summarized in terms of the diagrammatic representations of Figs. 1 and 2 [13, 15]. The mean crystallite size, the layer-plane orientation, and the angular distribution of mean crystallite size can be determined by X-ray diffraction methods, and the actual distribution of crystallite size can be determined by direct measurement on electron micrographs [16].

Reynolds and Sharp [17] suggest that, because structural restraints are imposed on the layer planes of misoriented crystallites, the shear stress induced parallel to the basal planes when tensile stress is applied to a fibre, can be sufficient to cause basal plane rupture in the misoriented crystallites. In effect, the concentration of shear strain energy in a misoriented crystallite is not relieved by cracks parallel to the layer planes, but by cracks at right angles. Once formed, a crack will propagate both across the basal plane, and, by transference of shear stress, through adjacent layer planes. This process is depicted schematically in Fig. 3. A misoriented crystallite (a), is put under tensile stress, basal-plane rupture occurs, and the crack propagates in the direction of $L_{a_\perp}$ and L_c (b), finally causing complete failure of the misoriented crystallite (c).

However, before a crack can propagate through a fibre and cause failure, either one of two conditions must be fulfilled.

1. The crystallite size in one of the directions of propagation of a crack, that is either $L_{a_\perp}$ or L_c, must be greater than the critical flaw size C for failure in tension.

2. The crystallite which initiates catastrophic failure must be sufficiently continuous with its

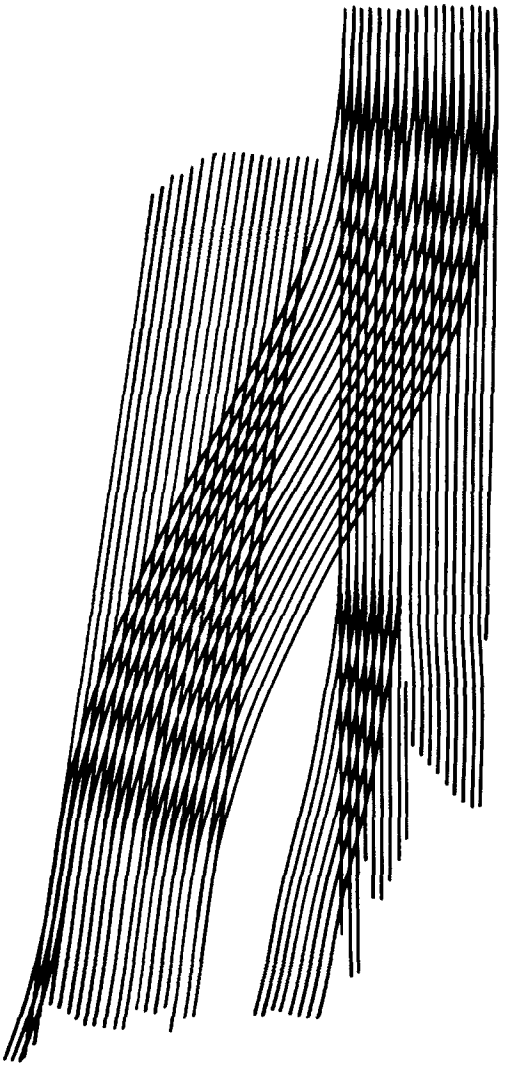

Figure 1 Schematic two-dimensional representation of longitudinal structure [13].

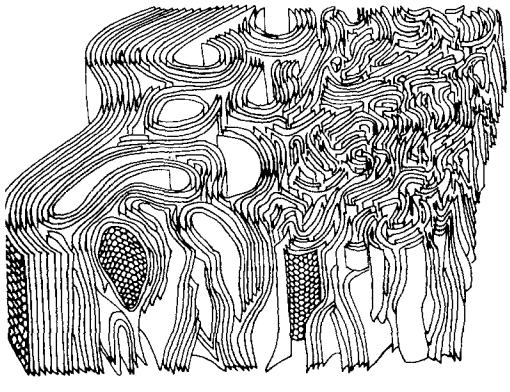

Figure 2 Schematic three-dimensional model of structure [15].

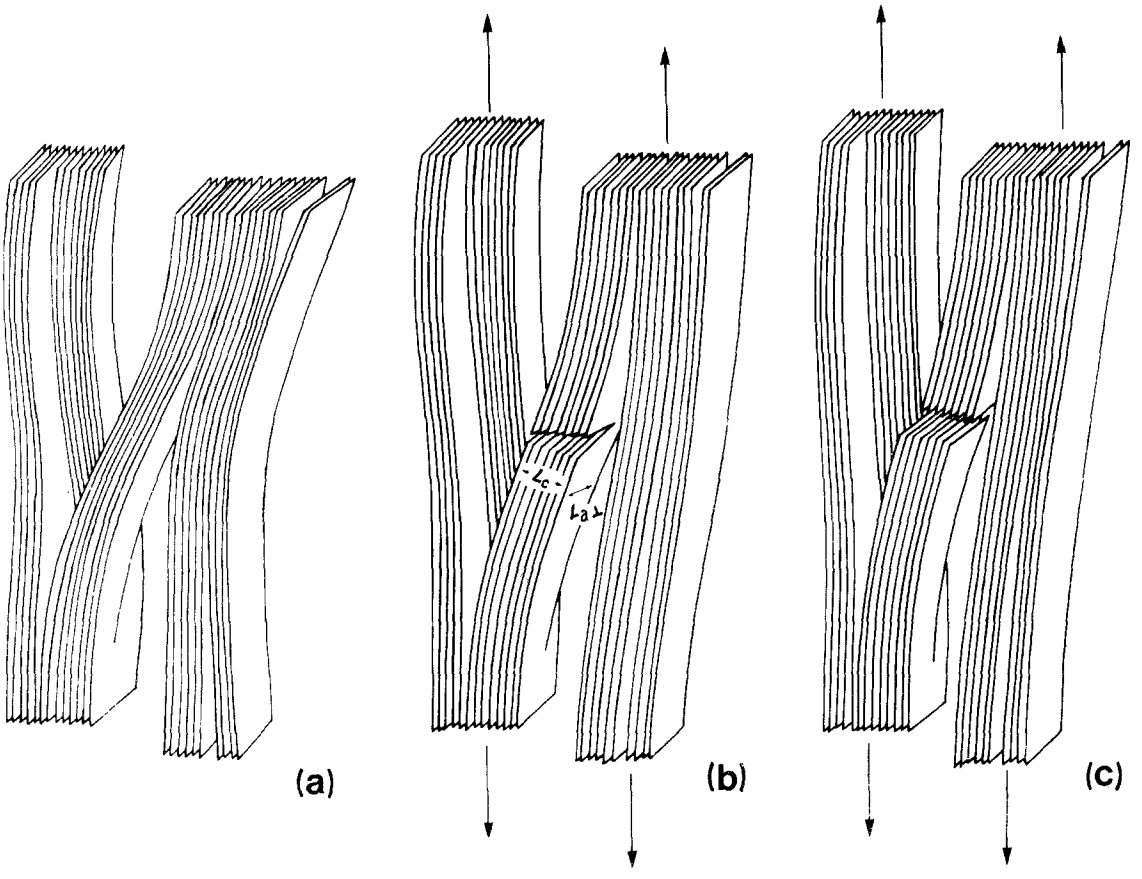

Figure 3 Reynolds and Sharp mechanism of tensile failure. (a) Misoriented crystallite linking two crystallites parallel to fibre axis. (b) Tensile stress exerted parallel to fibre axis causes basal plane rupture in direction $L_{a\perp}$, crack develops along $L_{a\perp}$ and L_c. (c) Further exertion of stress causes complete failure of misoriented crystallite. Catastrophic failure occurs if the crack size is greater than the critical size in L_c and $L_{a\perp}$ directions.

neighbouring crystallites for the crack to propagate.

The first condition is not normally fulfilled because both $L_{a_\perp}$ and L_c are much less than C. The second condition is most likely to be satisfied in regions of enhanced crystallization and misorientation around a defect.

In a misoriented crystallite, the effective compliance $s'_{\|}$, the strain per unit stress within a basal plane subjected to tension, increases rapidly with misorientation angle ϕ, the angle between the layer planes and the fibre axis.

$$s'_{\|} = s_{\|} \cos^4\phi + (s_{44} + 2s_{13}) \sin^2\phi \cos^2\phi + s_{33} \sin^4\phi \quad (2)$$

In the Reynolds–Sharp theory, the condition for tensile failure is

$$\frac{\sigma^2 s'_{\|}}{2} > \frac{\gamma_a}{\pi C} \quad (3)$$

$s'_{\|}$ will vary with the local value of ϕ and, since ϕ will sometimes be much greater than the mean misorientation, local conditions will exist where there is sufficient strain energy concentration to cause crack initiation at small defects. The initial crack, once formed, will propagate if there is sufficient continuity of structure to satisfy condition 2. Large crystallites can in fact be found in the recrystallized graphite which surrounds some flaws in carbon fibres; examples are shown later.

In a fibre, the crystallite shear strain-to-failure ϵ_s, can be calculated from

$$\epsilon_s = (\epsilon E/c_{44}) \sin\phi_c \cos\phi_c \quad (4)$$

where ϵ and E are the breaking strain and Young's modulus of the fibre respectively, c_{44} is the elastic constant for shear between the basal planes (4.0 GPa), and ϕ_c the local crystallite misorientation. If the local misorientation is at least twice

the mean misorientation, then for a Type II fibre with $E = 250$ GPa, $\epsilon = 1.5\%$, and mean misorientation = 6.1°, ϵ_s is about 20%, a value similar to that estimated from theory. By assuming that 20% is the intrinsic crystallite strain-to-failure in all fibres, Reynolds and Sharp calculated the intrinsic strain-to-failure, ultimate tensile strength (UTS), and critical flaw size (C), for other fibres (typically, UTS = 3.75 GPa and $C = 48$ nm for a Type II fibre, UTS = 4.80 GPa and $C = 42$ nm for a Type I fibre).

The present investigation is an attempt to characterize the mechanism of tensile failure by direct electron microscope observation in order to test the relevance of current efforts to determine practical and theoretical strengths of PAN-based and other carbon fibres. In this context, it is particularly important to test the validity of the Reynolds–Sharp theory in which crystallite size and orientation are the intrinsic factors which limit strain-to-failure and tensile strength.

2. Experimental details

PAN-based Type I carbon fibres with mean properties: diameter = 8.3 μm, UTS = 2.5 GPa and $E = 391$ GPa, were used for this investigation. The fibres were stressed to failure in glycerol by means of an Instron tensile test instrument using a 25 mm gauge length. The use of glycerol ensures that the broken ends are retained upon failure. The ends were washed free of glycerol in warm water and mounted on tabs of aluminium foil, which were then attached to specimen stubs with silver paste for examination in a scanning electron microscope (SEM). The ends were not coated with a conducting layer; they were examined at about x 5000 in the SEM, and the position of fracture initiation was either noted or photographed. Twenty fibres were tested and eleven pairs of ends were collected and examined. Two fibres were seen to have fractured from surface defects and none from internal holes. In order to mount in resin for sectioning and subsequent examination in a transmission electron microscope (TEM), a single fibre was cut from the SEM stub leaving a piece of foil attached to the fibre. The foil gave a reference so that, in the case of off-centre holes or surface defects, the fibre could be placed on a microscope slide with the defect nearest to the slide surface. The positioned end and its piece of foil were covered with a drop of the epoxy resin and the resin was hardened. The piece of resin containing the end was lifted from the slide, trimmed to remove the foil and excess resin, and mounted in more resin to form a block for cutting on the ultramicrotome.

Two of the fibre ends were mounted vertically for cross-sectioning. Longitudinal thin sections through the defects, together with transverse sections, were cut on an LKB ultramicrotome using a diamond knife and collected on 400 mesh copper grids covered with Formvar film. Many sections were cut but it was difficult to ensure that the sections landed clear of the grid bars as they were collected from the surface of the knife trough. Successful sections for TEM were cut from the fracture surfaces of three fibres only. These were fibre 14, UTS = 2.55 GPa; fibre 17, UTS = 2.48 GPa; fibre 18, UTS = 2.33 GPa. The sections were examined in a JEOL 100 CX transmission electron microscope under conditions which ensured that consecutive bright- and dark-field images could be recorded.

3. Results

3.1. Electron microscopy

Fig. 4 is a typical SEM image of a fracture surface used in the preparation of thin sections for TEM. Fig. 5 is a longitudinal section of fibre 18 seen in bright-field TEM. Fractography had revealed that there was a hole in the fracture surface, as in Fig. 4, but this hole was missed when longitudinal sections were cut. The micrograph shows another hole, 2 μm in width, below the fracture surface,

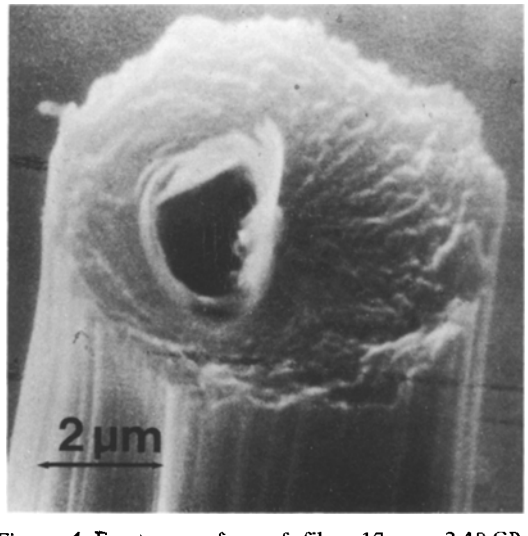

Figure 4 Fracture surface of fibre 17, $\sigma = 2.48$ GPa; graphitic sheets revealed in hole.

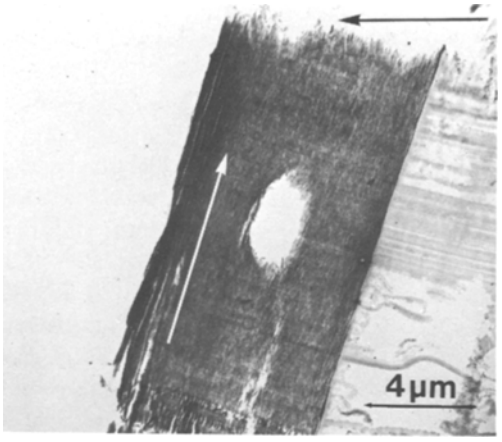

Figure 5 Fibre 18, $\sigma = 2.33$ GPa. Longitudinal section showing a hole in the fibre near the fracture face; this hole does not show an internal skin of graphite sheets. Black arrow – fracture face, white arrow – fibre axis.

which was only observed after cutting. This hole does not contain recrystallized graphite on its internal surface, but there are some crystallites, slightly larger than normal, lying in directions closely parallel to the fibre axis. Cross-sections were cut from the second end of fibre 18, and Fig. 6 shows that the fracture initiating hole was surrounded by large graphitic crystallites (arrowed).

Fractography showed that there was also a large off-centre hole in the fracture end of fibre 14. After longitudinal sectioning, a second hole was revealed below the fracture surface (Fig. 7). This hole contains crystallites which lie predominantly parallel to the fibre axis. The hole in the fracture end of fibre 14 is seen in Figs. 8a and b, which are a typical pair of bright-field and (0 0 2) dark-field micrographs. Fig. 9 depicts a section three cuts later, and shows a group of misoriented crystallites at high angles to the fibre axis (white arrow). The smooth nature of the surface suggests that this section has been cut through the fracture initiating region. The black arrows indicate equivalent regions of misoriented crystallites in the two sections.

Another fibre (fibre 17) failed at an internal flaw and yielded several interesting longitudinal sections. Three successive sections are shown in dark-field (0 0 2), as Figs. 10 to 12. The black arrow in Fig. 10 points to the surface of the defect containing a high proportion of large misoriented crystallites. The black arrows in Figs. 11 and 12 indicate cracks parallel to the fracture surface, which can be distinguished from the knife marks

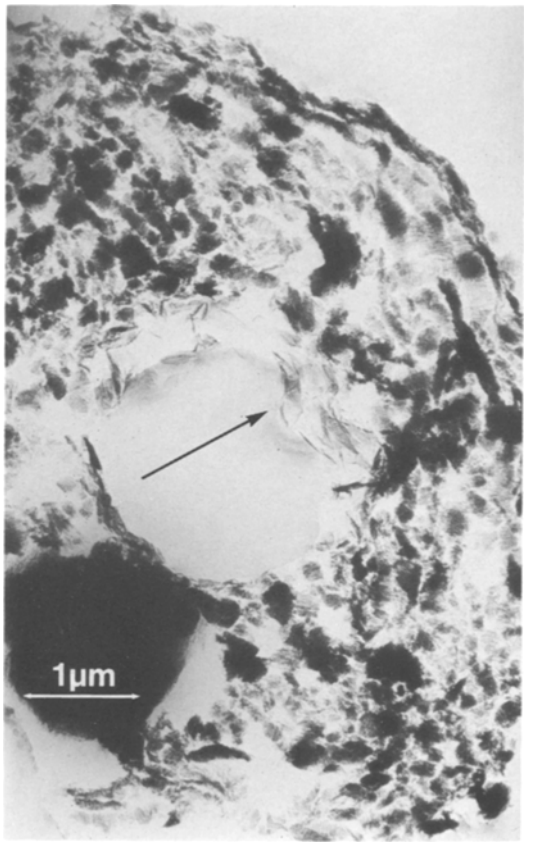

Figure 6 A transverse section through the hole in the other fracture end of fibre 18. This hole has a skin of graphite sheets and large crystallites (arrowed).

often seen on microtomed sections, since they do not extend into the embedding medium.

3.2. Reynolds–Sharp analysis

The fibre strain-to-failure as a function of crystallite misorientation is given in Fig. 13 for different values of E, as evaluated from Equation 4. The critical flaw size for a given ultimate tensile strength as calculated by the Griffiths Equation 1 is given in Fig. 14 for the same E values.

The mean crystallite size is a function of azimuthal orientation [1, 16]. Typically, L_c varies from 5.5 nm, for crystallites with layer planes oriented parallel to the fibre axis, to 2 nm for those at 40° to the fibre axis. If the mean crystallite size were the critical flaw size, then the intrinsic strength would be above 10 GPa. However, misoriented crystallites up to 20 nm in both L_c and $L_{a\perp}$ directions are not uncommon; this would be a critical flaw size for an intrinsic strength of 7.5 GPa at $E = 400$ GPa, which in turn

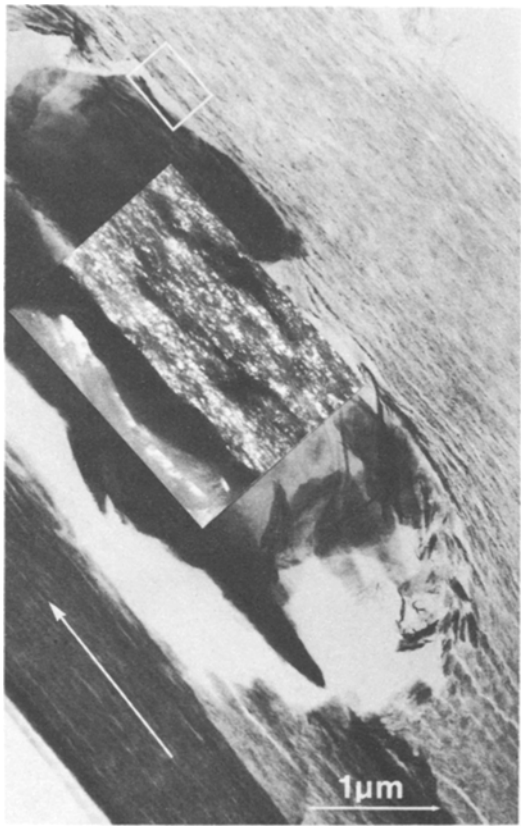

Figure 7 Fibre 14, $\sigma = 2.55$ GPa. The micrograph shows a hole near the fracture surface; this hole contains graphitic sheets and graphite crystallites which are predominantly parallel to the fibre axis. Failure was not initiated at this hole. White arrow – fibre axis; inset – dark field (0 0 2) (×4).

would imply a strain-to-failure of 1.9%. From Fig. 13 we note that this would be obtained at a misorientation of 6.5°.

It would seem reasonable to suggest that, if a Type I PAN-based carbon fibre is caused to fail by initiation from a single misoriented crystallite not associated with a discrete flaw, then 7.5 GPa is a good upper estimate of tensile strength at a modulus of 400 GPa. Lower intrinsic strengths must be expected in practice, because regions must exist within a normal fibre where propagation through a structural continuity can take place. Studies of lattice-fringe images of both transverse and longitudinal sections, suggest that the limit for continuity of crystallites in non-defect regions is about 50 nm, a value about ten times the mean crystallite size. We can see that, for a crystallite misoriented at 10° to the fibre axis, the average misorientation in a Type I fibre, a strain to failure of 1.3% can be expected at $E = 400$ GPa, reducing the tensile strength to 4.8 GPa, if the critical flaw size of 50 nm is exceeded by propagation of a crack through a structural continuity.

There is a high probability that single crystallites, or regions of crystallite continuity above critical size, and with twice the mean misorientation, are likely to be present in the walls of flaws. From Fig. 13, the strain-to-failure of a fibre with $E = 400$ GPa containing crystallites misoriented at 20° will be 0.6%, a UTS of 2.4 GPa. These greatly reduced properties are very similar to those of the fibres used in this work. Thus, a few large misoriented crystallites can result in a dramatic reduction in fibre strength.

4. Discussion

4.1. Tensile failure

Sharp and Burnay [5] were the first to point out that defect size may not be the determining factor in tensile failure, and that cracks may originate in the well graphitized lamellar structures found at the surface of the internal voids. The work reported here has demonstrated that tensile failure does not necessarily occur at the largest of neighbouring defects. It is clear that fibre 18 (see Fig. 5) did not break at the 2 μm hole shown in the micrograph, but through one of similar size seen in the cross-section (see Fig. 6) which contains sheets of well graphitized material with large crystallites. In fibre 14 (see Fig. 7) an intact hole below the fracture surface is shown, and, although it also contains well graphitized crystallites, fibre failure did not take place through the hole. It should be noted, however, that the layer planes are parallel to the fibre axis and the misorientation angle may have been insufficient to permit crack formation.

Micrographs such as Figs. 8 and 9 show that the growth of layer planes around some holes will provide regions where cracks can be formed at low stress levels, and where structural continuity exists through which a crack can propagate. In Fig. 8 the crystallites coating the hole in the fibre fracture surface can be seen to bend and follow the contour of the hole. Fig. 9 also shows that fracture was initiated in a region where crystallites are misoriented at high angles to the fibre axis. Again, Fig. 10, from the fracture end of fibre 17, shows that failure began in a region where there was a high proportion of misoriented crystallites.

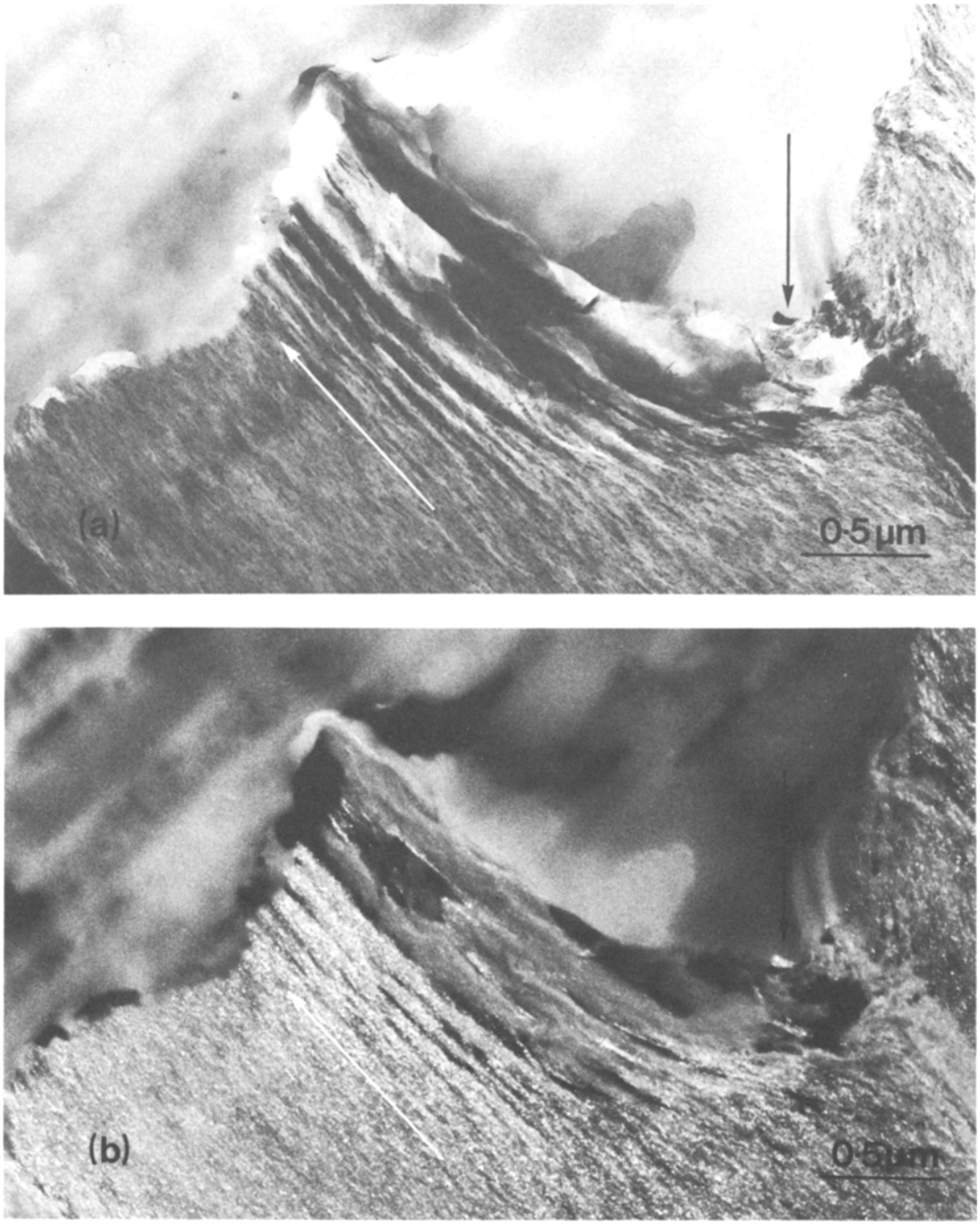

Figure 8 Fibre 14, the hole in the fracture surface, (a) bright-field, (b) dark-field (0 0 2), micrographs showing crystallites lining the hole. White arrow – fibre axis, black arrow – location of misoriented crystallites.

Carbon fibres have a notoriously low energy-absorbing capacity [9]. Evidence from Figs. 10 to 12 suggests the presence of an internal crack perpendicular to the axis of fibre 17 after failure. The energy liberated during tensile failure may well set up a longitudinal stress wave which, in the absence of an external damping medium such as glycerol, may cause the fibre to break up into several fragments.

These micrographs demonstrate that not all holes contained a coating of graphite-like sheets, those which did were probably the result of

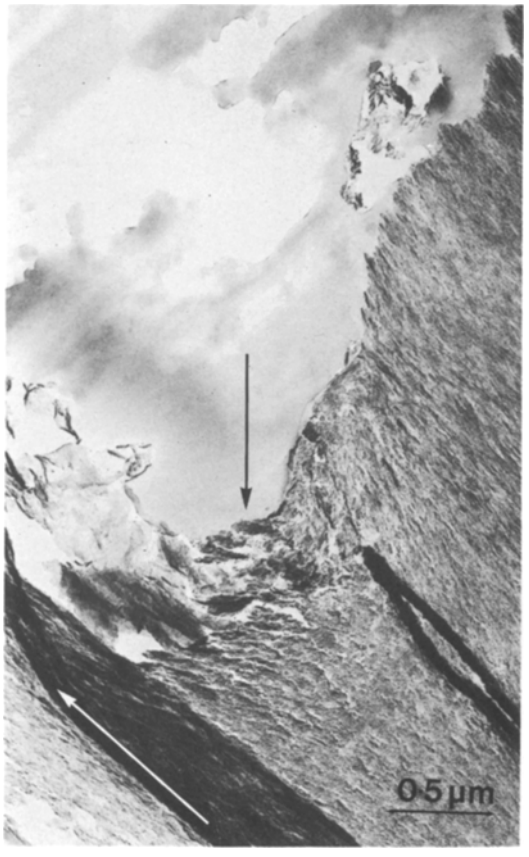

Figure 9 Fibre 14, a section three cuts away from that seen in Fig. 8 showing misoriented crystallites (black arrow) at high angles to the fibre axis (white arrow).

catalytic recrystallization [18] caused by a metal impurity. The hole with no recrystallized graphite (see Fig. 5) was probably a void in the original PAN fibre. Moreton and Watt [7] reported that, in order to increase fibre strength, the manufacturing process must be clean and free from impurities. The micrographs shown here emphasize that any impurities, particularly metals, which might cause recrystallization, must be rigorously excluded from the precursor polymer and carbon fibre manufacturing line.

Clearly, the presence of holes is not the true cause of low fibre strength, it is the presence of large misoriented crystallites surrounding some holes which has a deleterious effect on fibre strength. Large crystallites with layer planes parallel to the fibre axes do not initiate failure.

4.2. Ultimate tensile strength

The Reynolds–Sharp mechanism implies that the strength of fibres will increase if the orientation and hence the Young's modulus is increased. In fact Johnson [19] found that the strength of Type I fibres tended to increase from around 1.3 to 2.0 GPa, when the fibres were stretched 28% at 2800° C, a deformation which increased the Young's modulus from 403 to 656 GPa. There was considerable scatter in the strength results but this was probably due to the presence of holes and large misoriented crystallites in the fibres.

We have demonstrated the essential correctness of the Reynolds–Sharp mechanism for tensile failure in the case of Type I fibres, and suggest that if crack propagation is by a Griffiths mechanism alone, as depicted in Fig. 3, then an intrinsic fibre strength of 7.5 GPa can be expected in Type I fibres when $E = 400$ GPa. The presence of larger misoriented crystallites in continuity will reduce the effective strength. Assuming that a cleaner process will eliminate the cause of large misoriented crystallites, then the resulting improved distribution of layer–plane orientation should enable Type I fibres with a breaking strain of 1 to 1.3% to be made, that is an ultimate tensile strength of 4.0 to 5.2 GPa. Although this work is concerned only with Type I fibres, the reduced crystallite-size distribution found in Type II fibres should allow breaking strains in excess of 2% to be achieved.

Although a fibre does not always fail at the largest flaw, so-called weakest-link theories have been used to predict intrinsic carbon fibre strength since the gauge length dependence was reported by Moreton [2]. Chwastiak *et al.* [18] carried out a Weibull statistical analysis on mesophase pitch-based carbon fibres and predicted a strength of 5.3 GPa at 0.3 mm gauge length. A recent detailed analysis of flaws in similar fibres by Jones *et al.* [20] shows that careful spinning can eliminate large flaws, in which case surface pits become a limiting factor. The predicted tensile strength at 0.3 mm gauge length is then reduced to 3.8 GPa. Beetz [21, 22] has carried out a detailed Weibull analysis using the bimodal probability of failure as found with mesophase pitch-based fibres; this leads to a predicted strength of around 3.0 GPa at 0.2 mm gauge length.

The weakest-link approach to the calculation of intrinsic strength is essentially empirical in that it involves an extrapolation from data on defective material. The predicted strengths are very similar to, if slightly lower than, those suggested by a

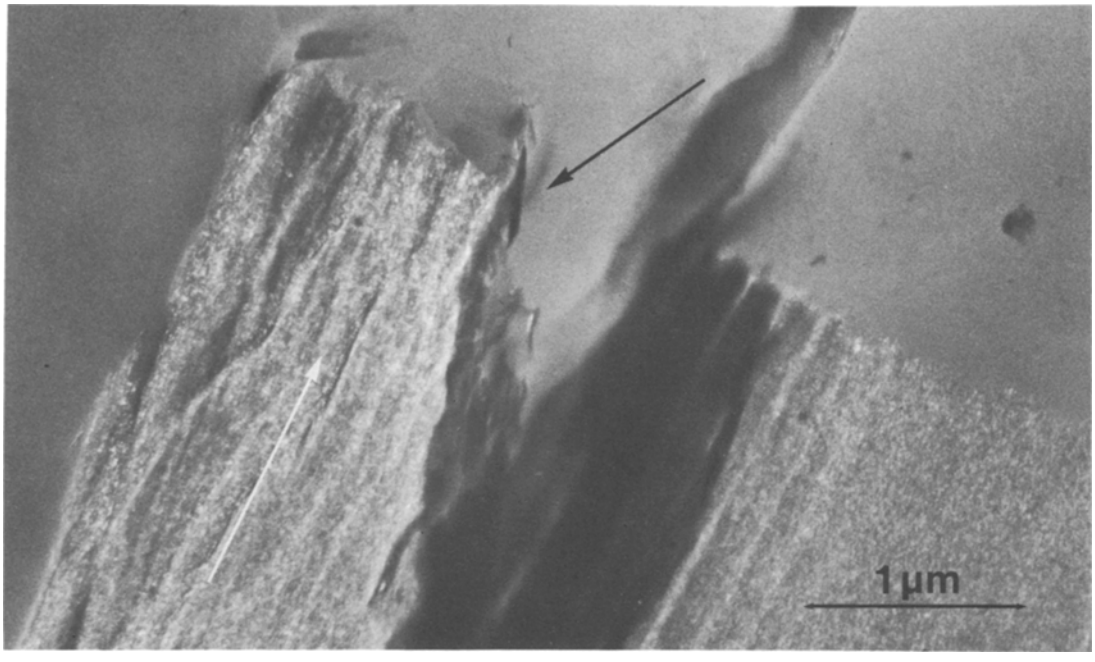

Figure 10 Fibre 17, section cut through the hole shown in Fig. 4. The hole is conical and here again crystallites (black arrow) can be seen at high angles to the fibre axis (white arrow).

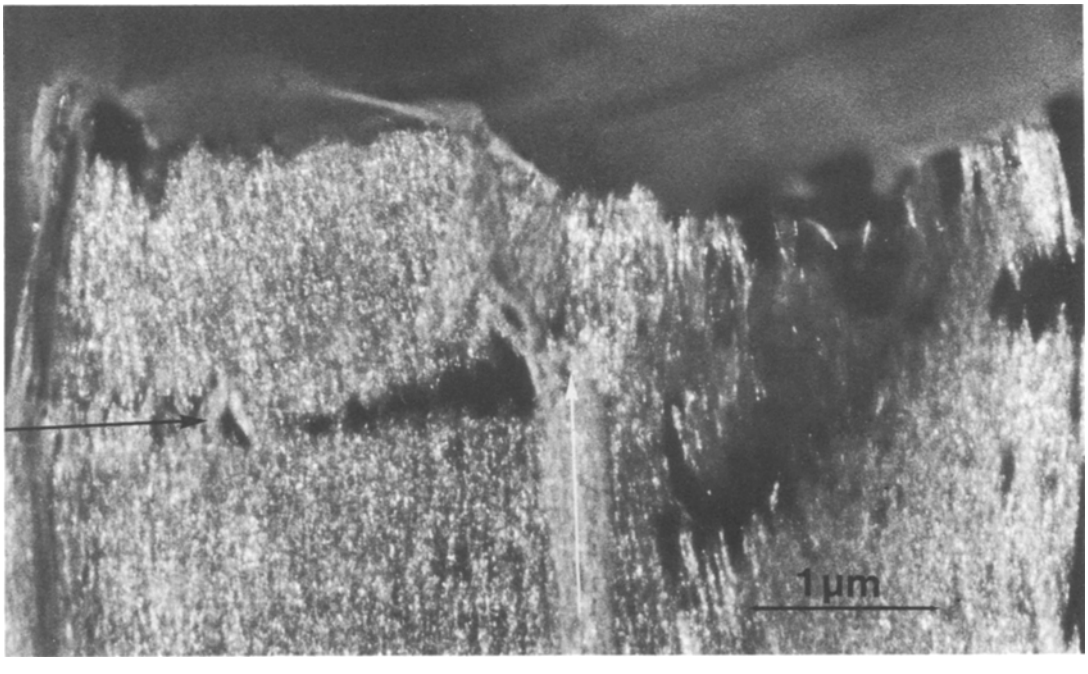

Figure 11 Fibre 17, next section to that of Fig. 10, shows the hole and an internal crack (black arrow) perpendicular to the fibre axis (white arrow) probably caused by energy liberated during tensile failure setting up a longitudinal stress wave.

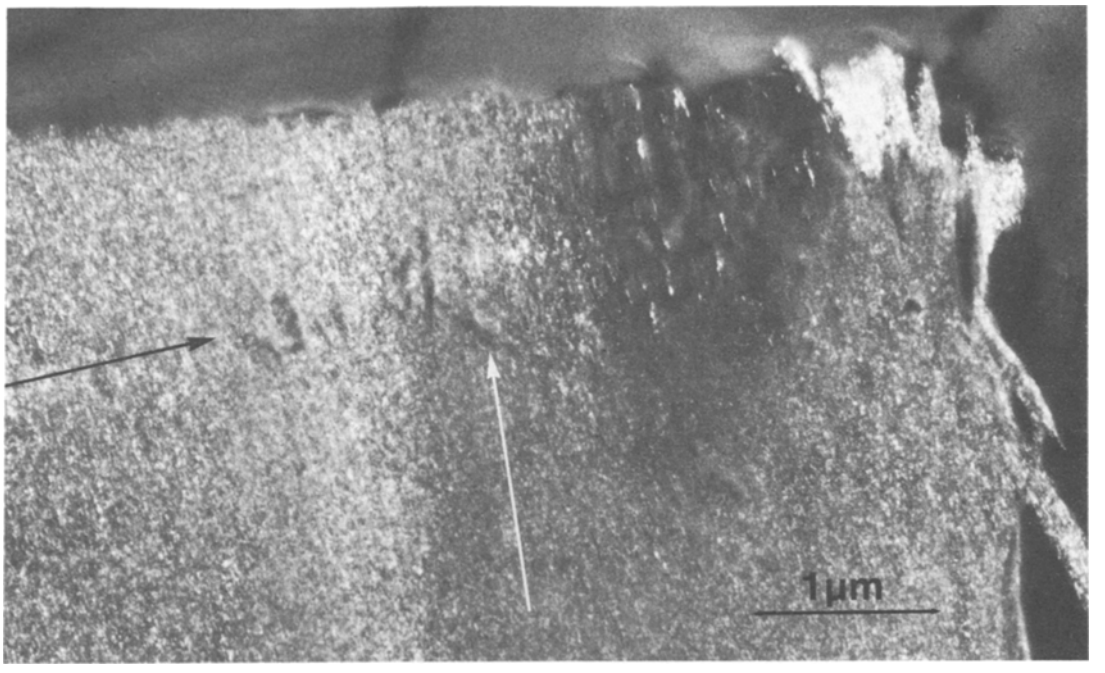

Figure 12 Fibre 17, next section to that of Fig. 11.

consideration of crystallite size and continuity, an indication that the two methods of prediction are converging. Essentially, we see that the weakest-link approach is influenced more by structure than is immediately apparent, and provides further proof for the correctness of the Reynolds–Sharp approach to tensile failure.

5. Conclusions

1. Holes in Type I fibres are not all equally effective as strength reducing flaws.

2. Tensile fracture is caused by the failure of layer planes in large misoriented crystallites which may be present around some holes. The mech-

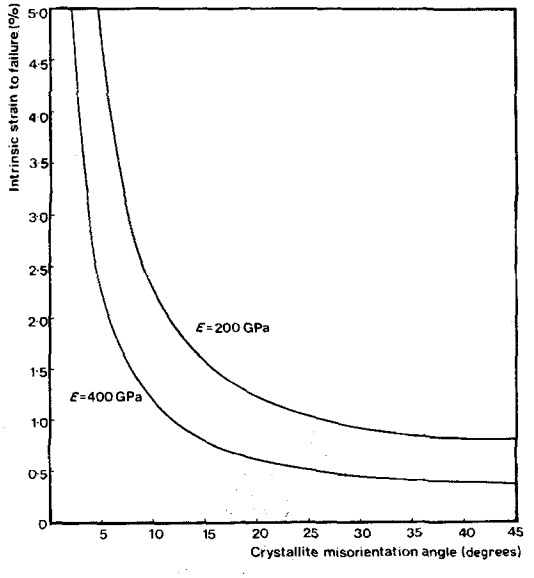

Figure 13 Intrinsic fibre strain to failure against crystallite misorientation angle, as evaluated by Equation 4 for different values of Young's modulus.

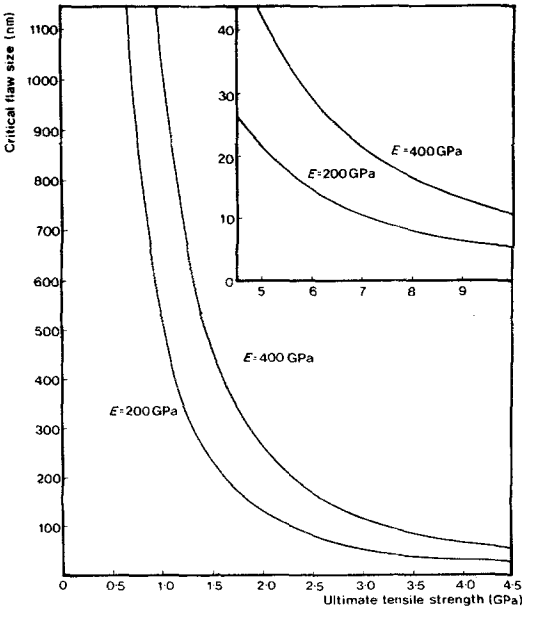

Figure 14 Critical flaw size against ultimate tensile strength, as evaluated by Equation 1 for different values of Young's modulus.

anism of failure is in keeping with the Reynolds–Sharp theory.

3. Clean precursors and working conditions to eliminate impurities should enable Type I fibres to be made with a breaking strain of 1 to 1.3%, and Type II fibres with a breaking strain greater than 2%.

Acknowledgements

The authors are grateful to Dr J. Harvey, RAE, for commenting on the manuscript. The work at Leeds was supported by the Procurement Executive, Ministry of Defence.

References

1. A. FOURDEUX, R. PERRET and W. RULAND, "Carbon Fibres: Their Composites and Applications" (Plastics Institute, London, 1971) p. 57.
2. R. MORETON, *Fibre Sci. Technol.* **1** (1968) 273.
3. J. W. JOHNSON, *Appl. Polym. Symp.* **9** (1969) 229.
4. J. W. JOHNSON and D. J. THORNE, *Carbon* **7** (1969) 659.
5. J. V. SHARP and S. G. BURNAY, "Carbon Fibres: Their Composites and Applications" (Plastics Institute, London, 1971) p. 68.
6. W. N. REYNOLDS, *Chem. Phys. Carbon* **11** (1973) 1.
7. R. MORETON and W. WATT, *Nature* **247** (1974) 360.
8. N. H. MACMILLAN, *J. Mater. Sci.* **7** (1972) 239.
9. G. DOREY, *Phys. Technol.* **11** (1980) 56.
10. D. J. JOHNSON, "Carbon Fibres: Their Composites and Applications" (Plastics Institute, London, 1971) p. 52.
11. D. CRAWFORD and D. J. JOHNSON, *J. Microsc.* **94** (1971) 51.
12. D. J. JOHNSON, D. CRAWFORD and B. F. JONES, *J. Mater. Sci.* **8** (1973) 286.
13. S. C. BENNETT and D. J. JOHNSON, *Carbon* **17** (1979) 25.
14. D. J. JOHNSON, *Phil. Trans. Roy. Soc. Lond.* **A294** (1980) 443.
15. S. C. BENNETT and D. J. JOHNSON, "Fifth London International Carbon and Graphite Conference" (Society of Chemical Industry, London, 1978) p. 377.
16. S. C. BENNETT, D. J. JOHNSON and R. MURRAY, *Carbon* **14** (1976) 117.
17. W. N. REYNOLDS and J. V. SHARP, *Carbon* **12** (1974) 103.
18. S. CHWASTIAK, J. B. BARR and R. DIDCHENKO, *ibid.* **17** (1979) 49.
19. W. JOHNSON, "Third London International Carbon and Graphite Conference" (Society of Chemical Industry, London, 1970) p. 447.
20. J. B. JONES, J. B. BARR and R. E. SMITH, *J. Mater. Sci.* **15** (1980) 2455.
21. C. B. BEETZ Jr, *Fibre Sci. Technol.* **16** (1982) 45.
22. *Idem, ibid.* **16** (1982) 81.

Received 14 February
and accepted 19 March 1983